

Chapter 8

Applications of UIH High-Resolution PET/CT in Zhongshan Hospital

Jun Zhou and Hongcheng Shi

Abstract With the advent of new generation high-resolution PET/CT (Shanghai United Imaging Healthcare Co., Ltd., UIH), the molecular imaging modality employed the cutting-edge lutetium-yttrium oxyorthosilicate (LYSO) crystal with size of 2.35×2.35 mm, which is of high stopping power, high light yield, and fast decay time, to gain adequate uniformity, excellent linearity, high resolution, and perfect alignment. When a PET/CT scanner is produced with high-resolution performance and time-of-flight technique, its clinical significance could be expressed as doctors can use a fine-resolution but sharp image to diagnose a fine and small tumor (e.g., to evaluate submillimeter pulmonary nodule) in the human body. The high-resolution time-of-flight PET/CT is a major advance with promise, which is very good news for nuclear medicine physicians and will enable us to respond to more clinical concerns with the superior technology.

With the advent of new generation high-resolution PET/CT (Shanghai United Imaging Healthcare Co., Ltd., UIH), the molecular imaging modality employed the cutting-edge lutetium-yttrium oxyorthosilicate (LYSO) crystal with size of 2.35×2.35 mm, which is of high stopping power, high light yield, and fast decay time, to gain adequate uniformity, excellent linearity, high resolution, and perfect alignment. When a PET/CT scanner is produced with high-resolution performance and time-of-flight technique, its clinical significance could be expressed as doctors can use a fine-resolution but sharp image to diagnose a fine and small tumor (e.g., to evaluate submillimeter pulmonary nodule) in the human body. The high-resolution time-of-flight PET/CT is a major advance with promise, which is very good news for nuclear medicine physicians and will enable us to respond to more clinical concerns with the superior technology.

UIH spared no effort to produce this high-resolution time-of-flight PET/CT scanner, which was soon installed in Zhongshan Hospital, Fudan University, in December 2014. Till to March 2016, 5000 patients performed examination using this high-

J. Zhou • H. Shi (✉)

Department of Nuclear Medicine, Zhongshan Hospital, Fudan University, Shanghai, China

Nuclear Medicine Institute of Fudan University, Shanghai, China

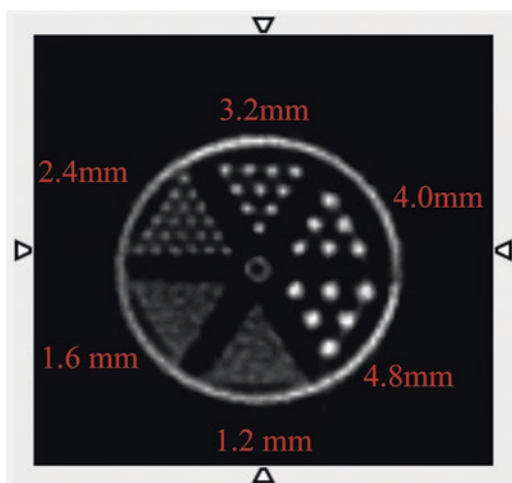
e-mail: shi.hongcheng@zs-hospital.sh.cn

resolution time-of-flight PET/CT scanner. Its clinical effect has been widely acclaimed for high temporal resolution (faster scan speed), high spatial resolution, high-quality image, and lower radiation dose. As a matter of fact, to be able to yield a high-resolution PET images, one PET/CT scanner needs (a) high-resolution detector, (b) appropriate physics corrections, and (c) advanced image reconstruction methods. The process of this scanner was validated before clinical application, and clinical evaluation was introduced as below.

8.1 Phantom Study

The image quality of UIH PET/CT was tested to surpass the industry's highest spatial resolution and the standard of the National Electrical Manufacturers Association (NEMA) of 2.8 mm in the spatial resolution. In the meantime, the temporal resolution achieved the industry-leading 486 picosecond. The uMI S-96R PET/CT alignment testing data and results showed that the dual modalities had a perfect match. The detector intrinsic uniformity testing suggested that both the percent variation and the asymmetry of the frequency distribution were very low. The spatial linearity testing demonstrated that the absolute linearity and the differential linearity are within perfect ranges. The spatial resolution and the energy resolution were tested with good results. The Mini Deluxe Phantom was used to evaluate ultrahigh-resolution PET, which showed that the rod diameter of 2.4 mm was clearly depicted (Fig. 8.1). The Hoffman brain phantom was performed to investigate acquisition and reconstruction methods by uMI S-96R PET/CT with good image quality (Fig. 8.2).

Fig. 8.1 Mini Deluxe Phantom tested by UIH PET/CT scanner



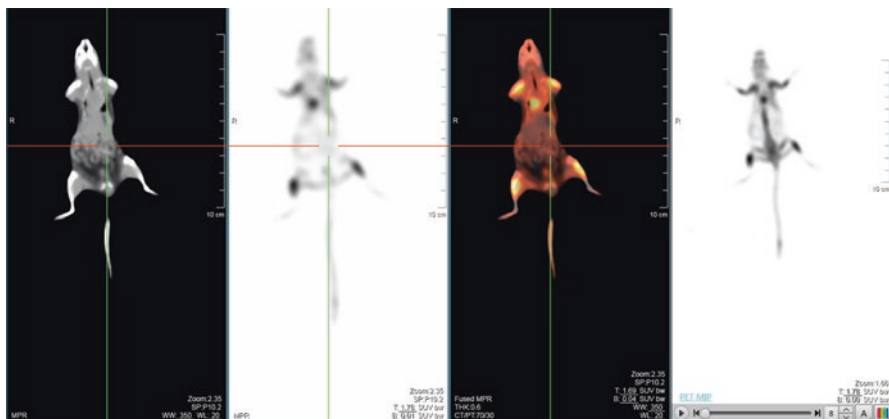


Fig. 8.3 (a–d) Normal mouse ^{18}F -FDG PET/CT imaging

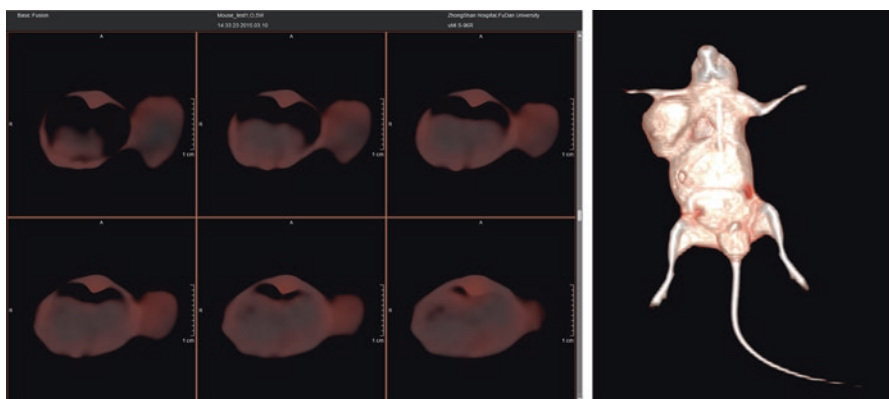


Fig. 8.4 (a–b) Tumor-bearing nude mouse ^{18}F -FDG PET/CT imaging

can easily detect fractures of the bilateral distal femoral bones of a dog prior to and after operation (Fig. 8.9a–d).

8.3 Clinical Evaluation

The UIH high-resolution time-of-flight PET/CT provided more doctor-friendly information in oncology, infection, and cardiovascular diseases. The clinical oncology applied PET/CT to diagnose tumor, to search for unknown primary malignant tumor, to perform tumor staging and restaging, and to evaluate therapy response.

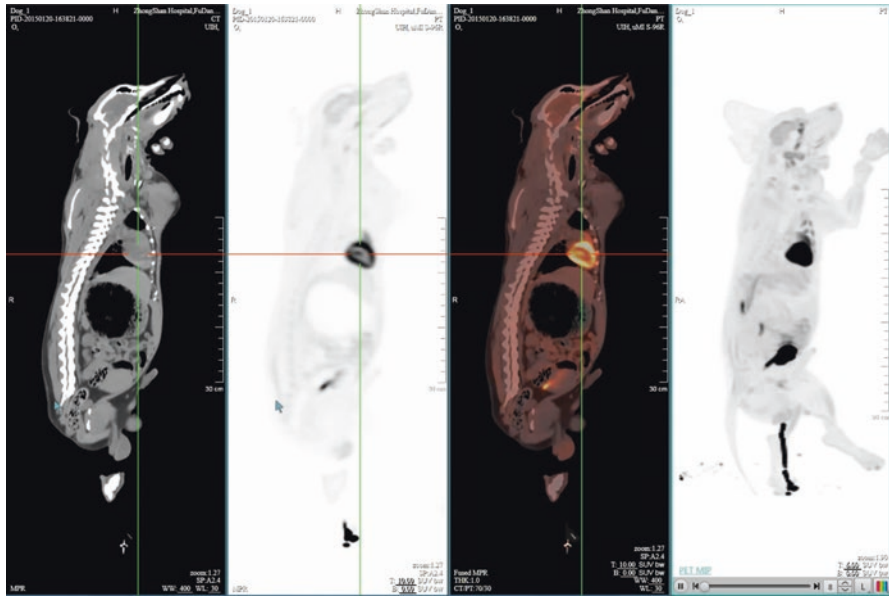


Fig. 8.5 (a-d) ¹⁸F-FDG dog whole body imaging

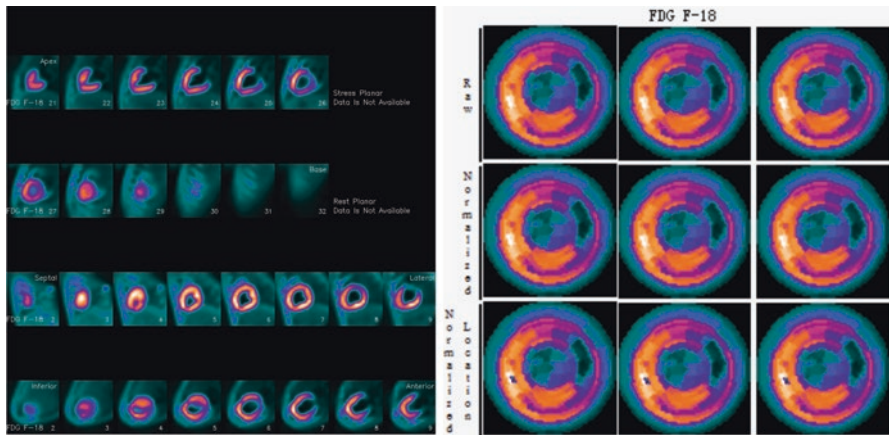


Fig. 8.6a-b ¹⁸F-FDG dog heart imaging

(1) There are several cases (including lung cancers, gastric cancer, and pleural mesothelioma) to show the clinical implication of the high-resolution time-of-flight PET/CT.

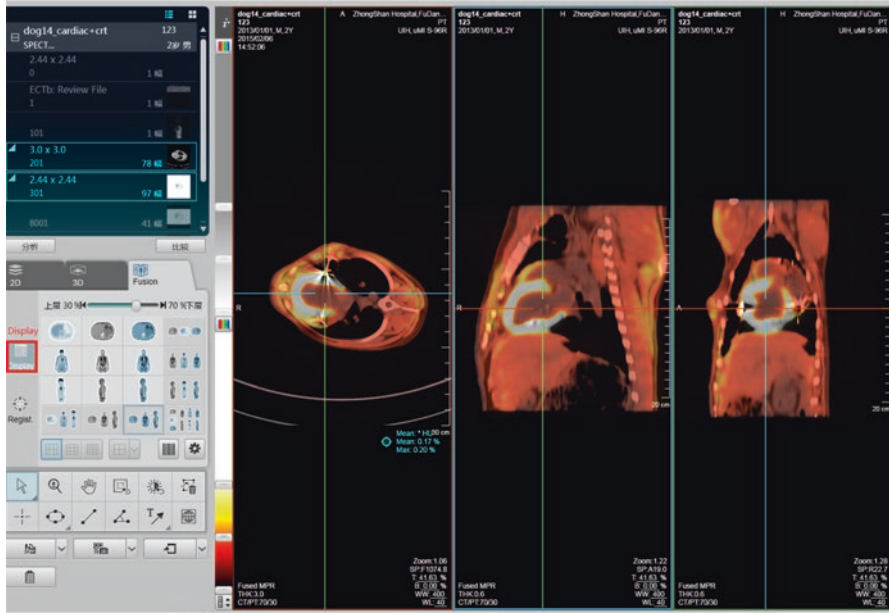


Fig. 8.6c–e Fusion tools for ^{18}F -FDG PET/CT – display with dog heart

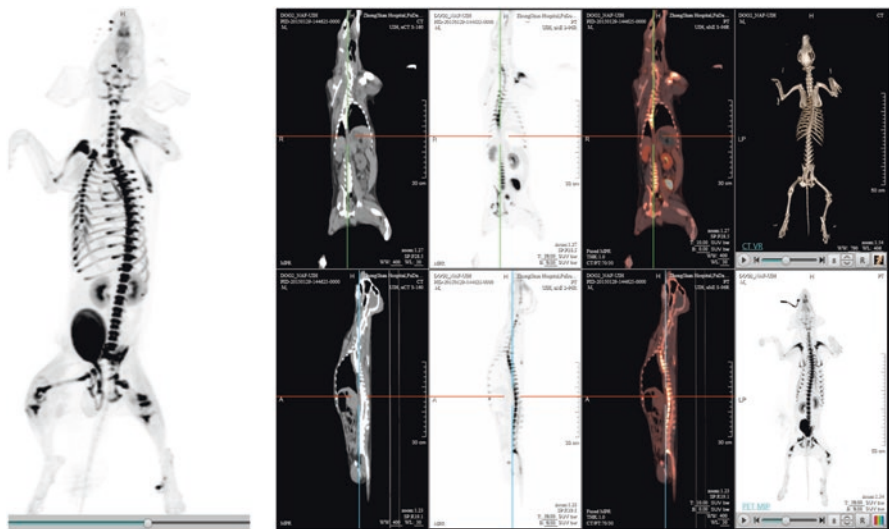


Fig. 8.7 (a–i) ^{18}F -NaF dog whole body bone imaging

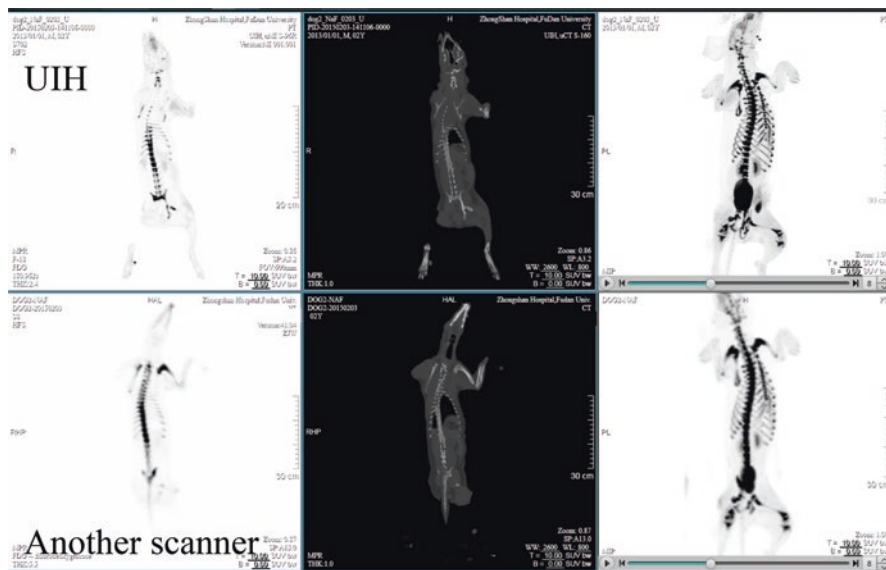


Fig. 8.8 (a-f) ^{18}F -NaF dog whole body bone imaging

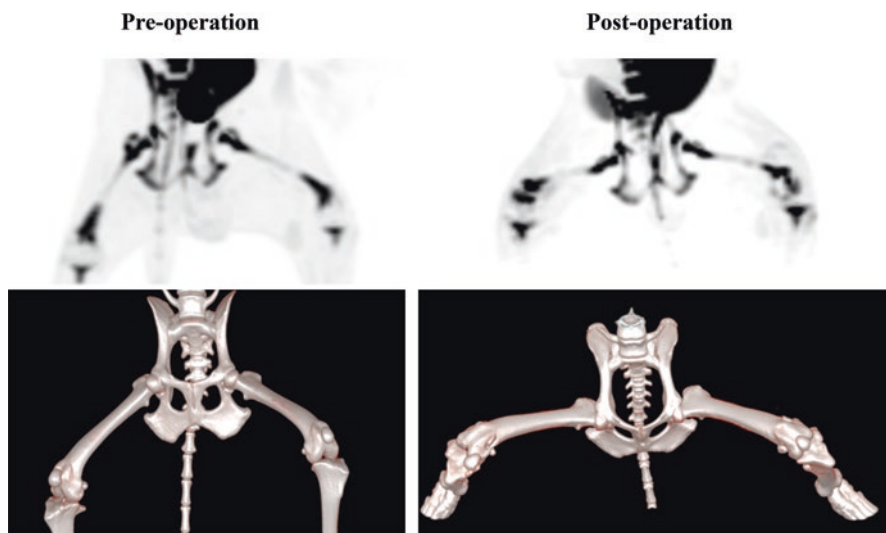


Fig. 8.9 (a-d) ^{18}F -NaF dog bone imaging with the bilateral distal femoral fractures

Case 1: A 51-year-old woman presents with no fever and cough (Figs. 8.10a–b and 8.10c–f).

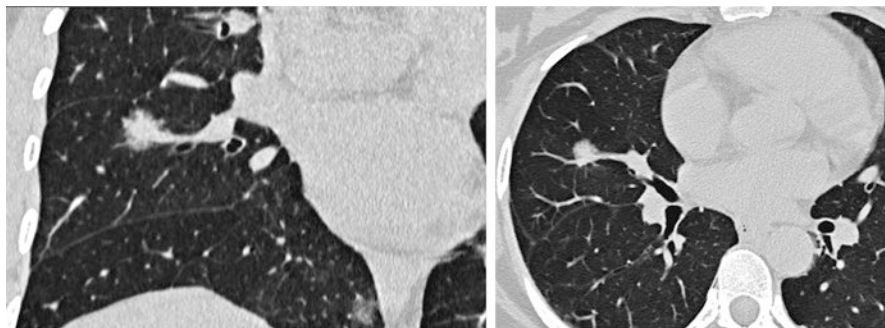


Fig. 8.10a–b CT images on lung window showed an oval, spiculated, mixed ground-glass opacity nodule at the middle lobe of the right lung

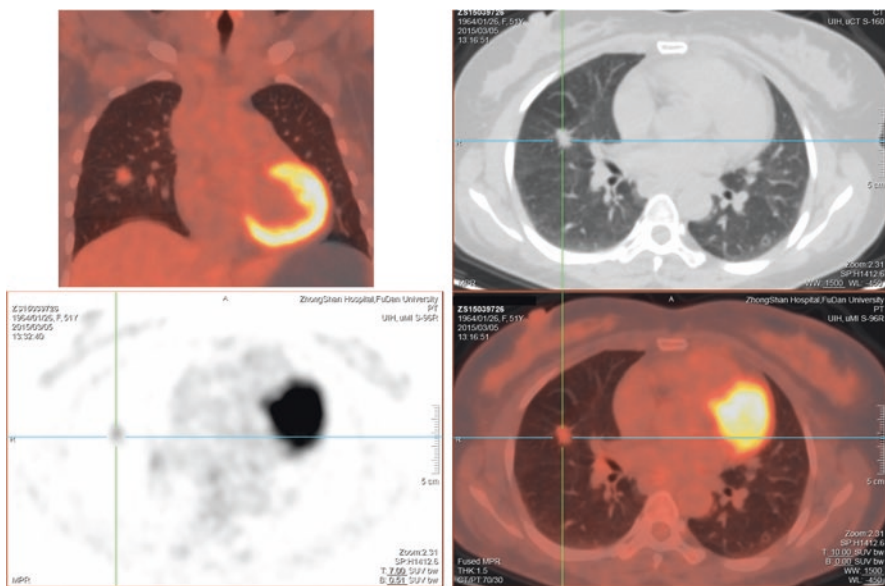


Fig. 8.10c–f ^{18}F -FDG PET/CT was performed for differential diagnosis of a solitary pulmonary nodule. PET/CT images with MPR demonstrated that the solitary pulmonary nodule was of marked FDG uptake with 2.37 of SUVmax and 0.58 of SUVmean. The nodule was pathologically confirmed to be a Grade II alveolar type lung carcinoma

Case 2: A 74-year-old man presents with stimulating dry cough, chest tightness, and shortness of breath for a week (Figs. 8.11a–c and 8.11d–l).

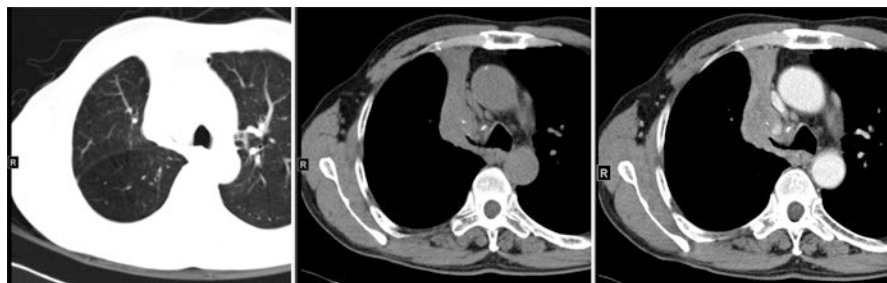


Fig. 8.11a–c Axial non-enhanced chest CT images on lung window (2A) and mediastinal window (2B) showed marked tapering and obstruction in the initial segment of the bronchus of the right upper lobe. Axial contrast-enhanced chest CT scan (2C) showed a segmental atelectasis of the right upper lobe caused by a mass in the right hilum. ^{18}F -FDG PET/CT was performed for differential diagnosis of the mass

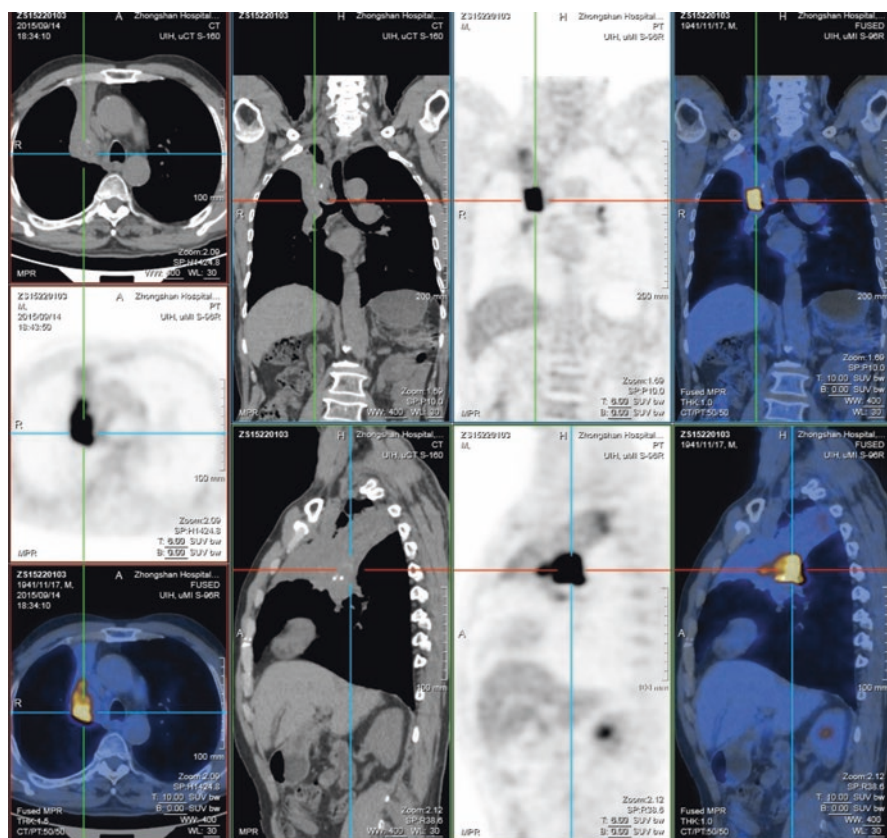


Fig. 8.11d–l PET/CT images with MPR demonstrated that the right hilar mass was of marked FDG uptake. Lung cancer was confirmed by fiber-optic bronchoscopy with biopsy. Then, a right upper lobectomy was performed, and the mass was pathologically verified to be squamous cell carcinoma. Two lymph node metastases were found in a regional lymph node dissection

Case 3: A 66-year-old man presents with a persistent stomachache for 2 months (Fig. 8.12).

Case 4: A 46-year-old man presents with serious chest pain (Fig. 8.13).



Fig. 8.12 (a–c) An axial non-enhanced upper abdominal CT image with prone position (a) displayed a focal thickening with ulcerative appearance in the lesser curvature of gastric wall. An axial contrast-enhanced upper abdominal CT scan with supine position (b) showed marked enhancement of the mass in the lesser curvature of gastric wall. Then, the patient underwent gastroscopy and three ulcer lesions were found within the wall of stomach. PET/CT scan was performed for tumor staging. PET/CT fusion image with prone position (c) showed the ulcerative mass was of marked FDG uptake. The mass was pathologically verified to be a poorly differentiated ulcer-type adenocarcinoma

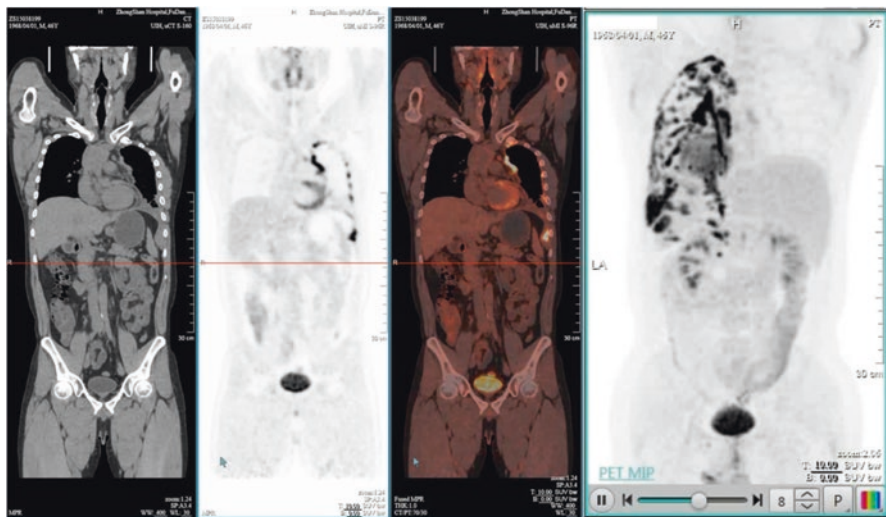


Fig. 8.13 (a–d) A coronal non-enhanced CT image (a) demonstrated diffuse left pleural thickening with a small amount of effusion. ^{18}F -FDG PET/CT was performed for differential diagnosis and staging. Coronal PET image (b), PET/CT image (c), and PET image with maximum intensity projection (d) demonstrated that marked diffuse FDG uptake lesions were noted within the left pleural cavity and peritoneal cavity. Malignant mesothelioma of pleura and peritoneum was presumed, and the outpatient patient rejected a further diagnosis

(2) Searching for unknown primary malignant tumor is another wonderful clinical application for PET/CT. We can take another two cases for example.

Case 5: A 62-year-old man who has a lump with gradual enlargement in his right neck for 3 months presents with no history of malignancy. Chest CT scan showed nothing significant (not shown). Gastroscopy was performed and no malignant evidence was found. PET/CT scan was applied for searching primary tumor (Fig. 8.14).

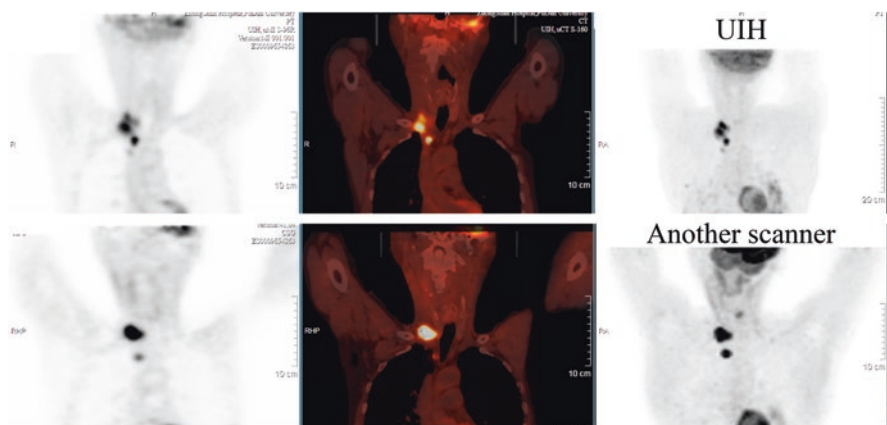


Fig. 8.14 (a–f) The top three UIH coronal PET/CT images (a–c) showed that multiple lymphadenopathies with marked FDG uptake were well displayed with specific morphological features, which is superior to the bottom three coronal PET/CT images (d–f) with 1 h delay scan from another scanner. The right upper mediastinal mass was pathologically verified to be a poorly differentiated thyroid carcinoma

Case 6: A 65-year-old man with unexplained syncope underwent brain MRI examination. Multiple metastatic lesions were founded on MRI (not shown). PET/CT was performed for searching for an unknown primary tumor (Fig. 8.15).

(3) Tumor staging (e.g., breast cancer, ovarian cancer, and liposarcoma) and tumor restaging after therapy are one of the most important clinical applications for PET/CT.

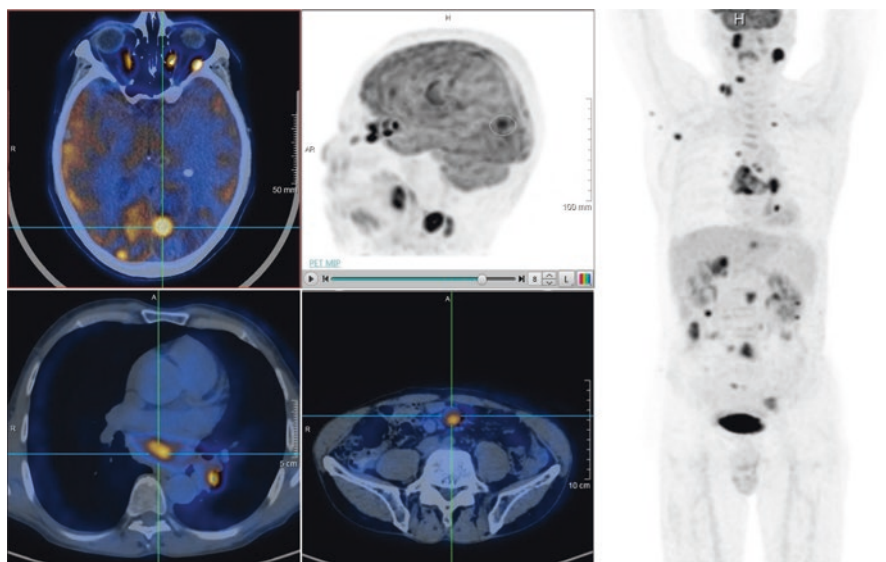


Fig. 8.15 (a–e) PET/CT and PET MIP images showed that multiple marked FDG uptake mass was identified in the bilateral occipital lobes, the bilateral necks, the right axillary fossa, the bilateral hilar regions, the mediastinum, the mid-lower esophagus, and the peritoneal cavity. The lesions were pathologically verified to be small cell carcinoma and mixed squamous cell carcinoma

Case 7: A 55-year-old woman presents with lower abdominal pain and increased stool frequency recently. The patient also reports about 3 kg weight loss within last 1 month. Abdominal ultrasonography demonstrates bilateral ovarian masses, uterine leiomyoma, and a small amount of fluid accumulation in the pelvic cavity. PET/CT scan was applied for diagnosis and staging (Fig. 8.16).

Additional Findings Laparoscopic examination showed a 4 cm*4 cm*3 cm soft tissue mass in the left ovary. The right ovary adhered to adjacent organs, the greater omentum looked like biscuits, and diffuse miliary nodules were seen on the surface of the liver.

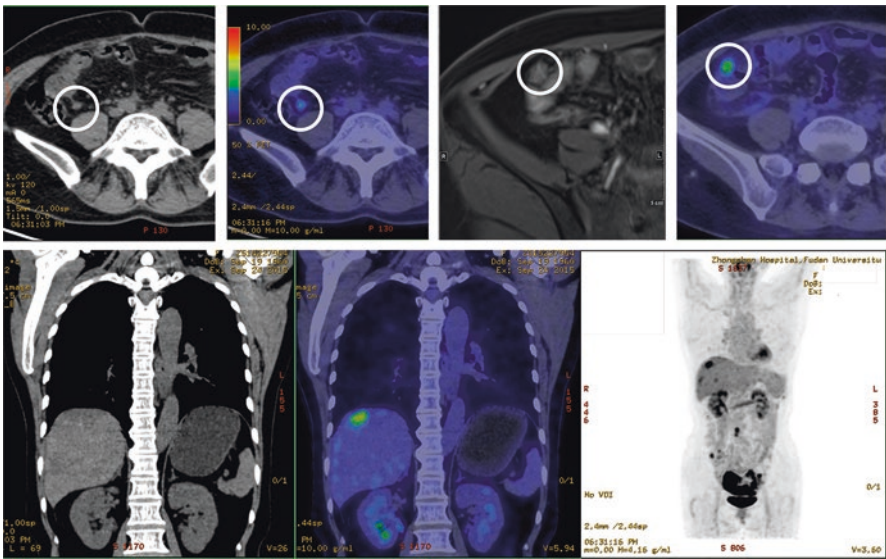


Fig. 8.16 (a–g) Axial lower abdominal CT image (a) and PET/CT image (b) demonstrated that an enlarged lymph node (within *white circle*) with increased FDG uptake was noted in the ileocecal region. Axial contrast-enhanced lower abdominal MRI image (c) and PET/CT image (d) showed that an enlarged lymph node (within *white circle*) was seen adjacent to the right anterior peritoneum. Coronal non-enhanced CT image and PET/CT image (e–f) showed that a large low density mass with markedly increased FDG uptake was identified in the right lobe of liver. Coronal PET image with maximum intensity projection showed that multiple masses with lymphadenopathies were revealed in the entire abdomen

Case 8: A 35-year-old man underwent a mass resection of the right leg for suffering from myxoid liposarcoma. Recent CT imaging found suspected metastatic lesions in the bilateral lungs. PET/CT scan was performed for staging (Fig .8.17).

Case 9: A 50-year-old woman presents with a right breast mass (Fig. 8.18).

(4) The tumor therapy response evaluation based on PET/CT is a more feasible and reliable method at the present day. Especially, surveillance of molecular targeted tumor treatment is one of the most important clinical significance for PET/CT, which is a prognostic tool to tumor management in the past decade.

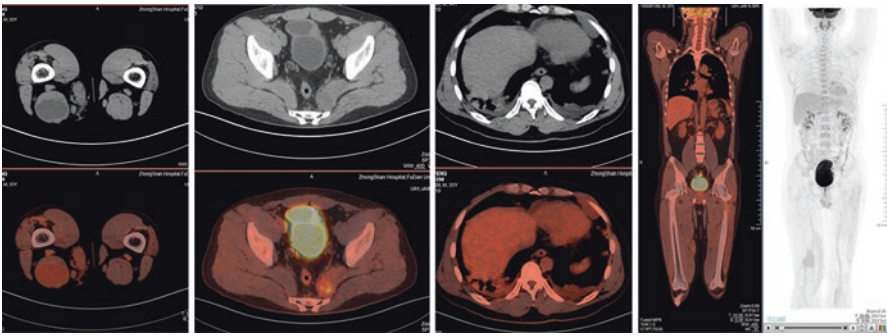


Fig. 8.17 (a–h) PET/CT images (a–h) demonstrated a well-defined, homogeneous high FDG uptake, and mixed solid and cystic myxoid liposarcoma behind the right distal femur prior to tumor resection, and an ill-defined, heterogeneous high FDG uptake, and low density soft tissue mass in the left pelvic cavity and multiple high FDG uptake pulmonary nodules in the bilateral lungs with bilateral pleural effusions

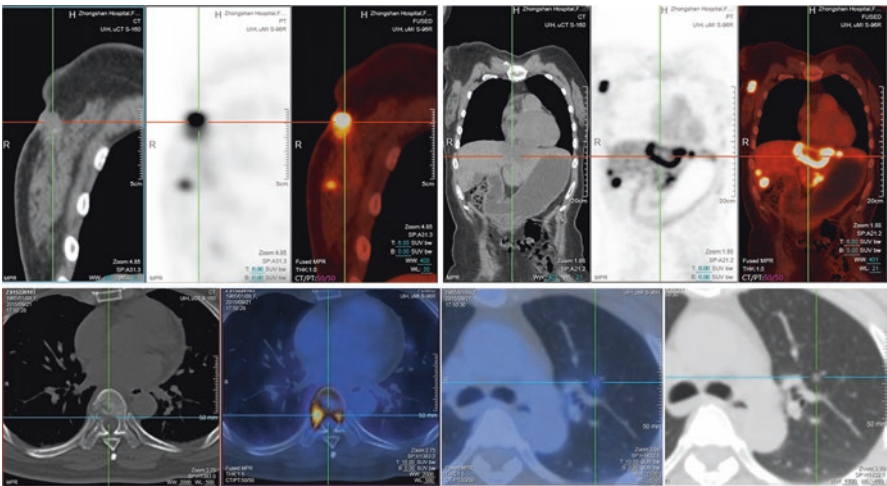


Fig. 8.18 (a–j) PET/CT scan was applied for diagnosis and staging. PET/CT images with multiplanar reformat (a–j) demonstrated an ill-defined, high FDG uptake, and soft tissue mass in the right breast with retraction of the adjacent skin, a moderate FDG uptake pulmonary nodule, multiple high FDG uptake masses in the liver, and multiple high FDG uptake osteolytic lesions within the thoracic vertebrae

Case 10: A 59-year-old man who was diagnosed with lymphoma half a year ago. PET/CT was performed again for therapy response evaluation and restaging after systemic chemotherapy (Fig. 8.19).

Case 11: A 38-year-old man was diagnosed with diffuse large B cell type non-Hodgkin’s lymphoma of the left tonsil. ¹⁸F-FDG PET/CT was performed for staging before therapy and for therapy response evaluation after three-cycle chemotherapy (Fig. 8.20).

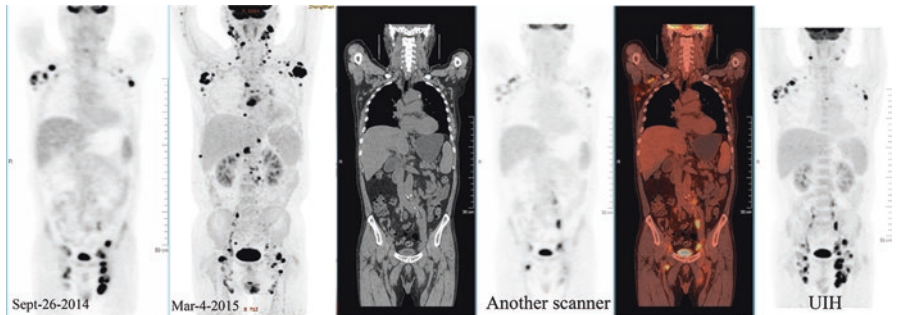


Fig. 8.19 (a–f) Coronal PET/CT images demonstrated that multiple high FDG uptake soft tissue masses or lymph nodes were noted in the bilateral axillary fossae and the bilateral inguinal fossae on September 26, 2014 (a), and then lymphoma progressed to the bilateral neck, mediastinum, peritoneal cavity, and the surface of liver on March 4, 2015 (b), although several lesions in the bilateral inguinal fossae disappeared after treatment (10B). The coronal PET/CT images (c–f) showed that multiple lymphadenopathies with marked FDG uptake before systemic chemotherapy. The UIH PET MIP image (f) well displayed multiple lymphadenopathies with specific morphological features, which is superior to the PET MIP image from another scanner

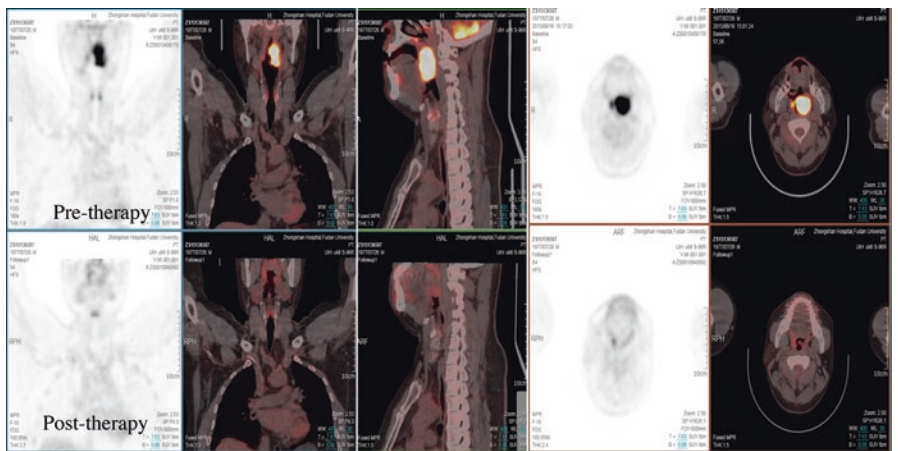


Fig. 8.20 (a–j) PET/CT images with MPR demonstrated that a large, high FDG uptake, soft tissue mass was seen in the left tonsil (a–e), and the mass vanished after treatment for non-Hodgkin’s lymphoma (f–j)

- (5) Infection is a common disease in clinical settings. Most of infectious diseases may manifest as marked high FDG uptake such as tuberculosis, lung abscess, aspergillosis, bacterial pneumonia, and so forth.

Case 12: A 61-year-old man accepted aortic valve replacement operation in April 2014. The patient felt swelling and pain in the region of chest incision 4 months later after operation. Incision and drainage operation was performed in October 2014. The patient felt even worse swelling and pain in the region of chest incision again 1 year later after operation (Fig. 8.21a–c). Skin ulceration appeared and pus outflow was found soon. PET/CT scan was performed for evaluating infection lesions (Fig. 8.21b–d). Infection focus removal operation was performed. Acute and chronic inflammatory cell infiltrations as well as microabscesses were found in the removal chest wall.

Case 13: A 62-year-old woman accepted total arch replacement and descending aorta intraluminal stent grafting for suffering type A dissecting aneurysm. The swelling and pus outflow in the region of chest incision were found repeatedly. Exploration of the infection of the aortic vascular prosthesis and reconstruction of

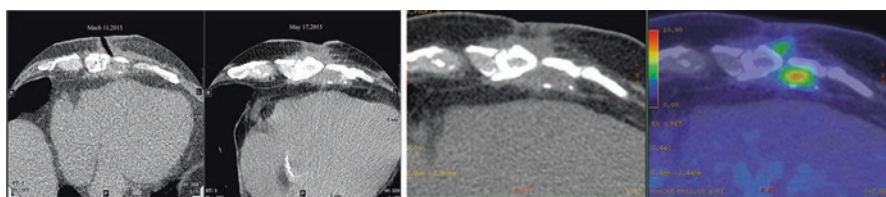


Fig. 8.21 (a–d) Pre-contrast CT scan images (a–b) with mediastinal window showed persistent infection in the region of lower sternum within 1 year after operation. PET/CT images revealed the severity and the extent of infection, which were displayed hot spots

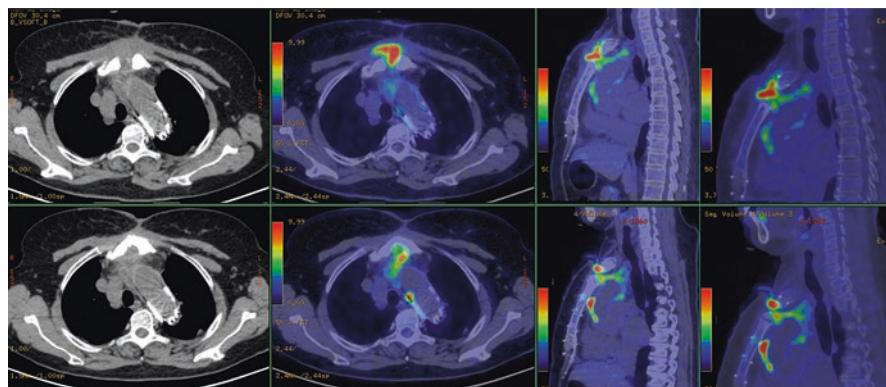


Fig. 8.22 (a–h) The top four PET/CT images (a–d) showed that multiple marked FDG uptake lesions, which severity of infection is lower than that of the bottom four PET/CT images after intervention (e–h), were seen in the region of chest incision and mid-anterior mediastinum

chest wall with muscle flap transfer were performed in May 2015. PET/CT scan was performed for evaluating infection lesions before therapy and evaluating the therapy response after therapy. Pathology was verified to be chronic inflammatory cell infiltration and giant cell reaction was found in the removal chest wall (Fig. 8.22).

- (6) As a very important method for diagnostics and assessment of prognosis in ischemic heart disease, the clinical value of PET/CT is gradually getting much attention in cardiovascular disease.

Case 14: A 54-year-old man was performed PCI in ER for suffering from ACS. Coronary artery angiography showed that 95 % stenosis was noted in the middle segment of the left anterior descending branch with blood thrombosis, 75 % stenosis in the middle segment of the first diagonal branch, and 80 % stenosis in the proximal segment of the second diagonal branch of the LAD coronary artery. A stent was input in the middle segment of the LAD after thrombus aspiration. Myocardial perfusion and FDG imaging were performed for evaluating myocardial viability (Fig. 8.23).

Summary UIH PET/CT scanner in Zhongshan Hospital is widely used in clinical settings. The high-resolution time-of-flight PET/CT scanner can provide high-quality diagnostic imaging. By now it is stable for use, and its scan time is also reasonable. Moreover, the HyperView (23.6 cm) is convenient to use for patients. In addition, the scanner for small animal study is extra benefits. We think that the UIH high-resolution time-of-flight PET/CT scanner will be widely used in clinical practice and benefit more patients with promise.

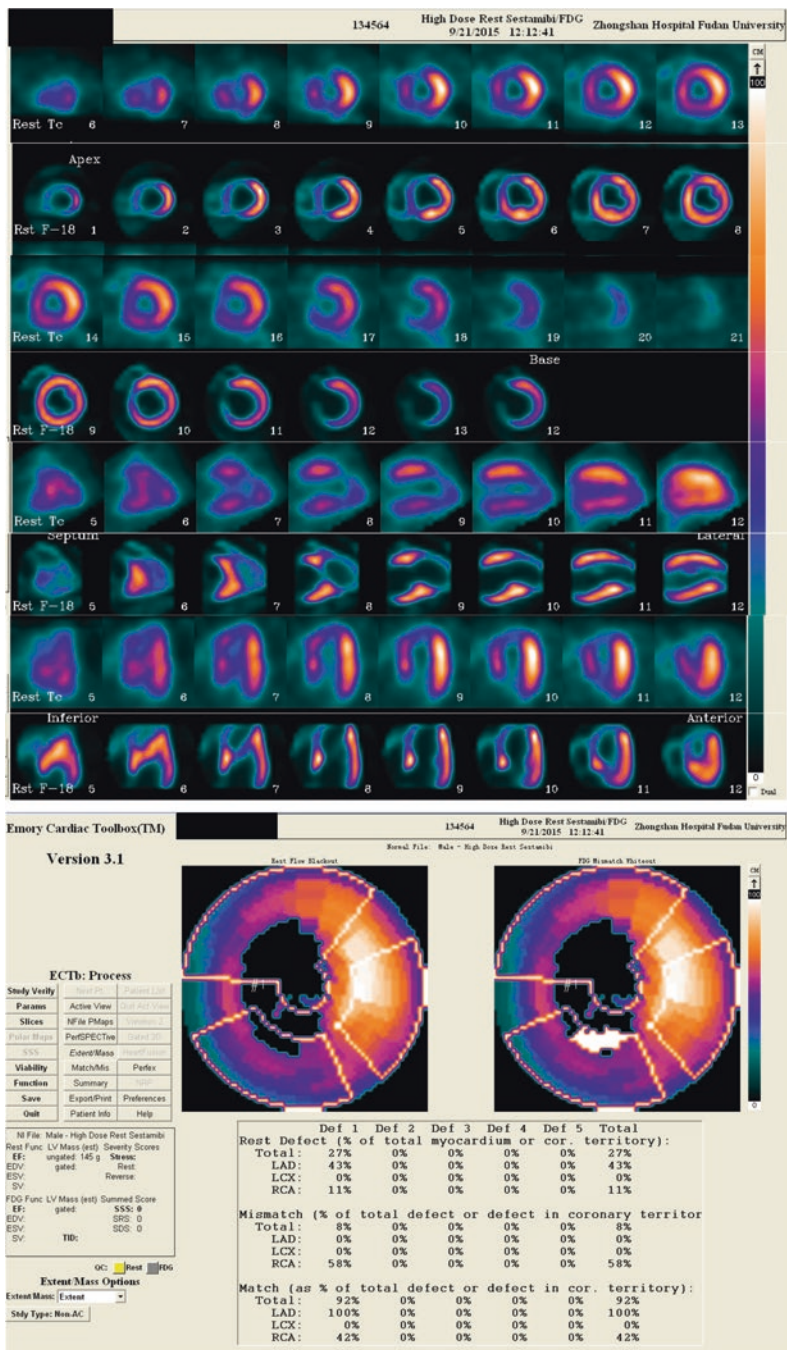


Fig. 8.23 (a-b) Resting myocardial ¹⁸F-FDG PET perfusion imaging perfectly matched with ^{99m}Tc-sestamibi cardiac scan images (a). The defects in the anterior and inferior wall, anterior and septal walls at the apex, and apex were seen in the left anterior descending territory (b)